Predicted High-Pressure Hot Superconductivity in Li_2CaH_{16} and Li_2CaH_{17} Phases that Resemble the Type-II Clathrate Structure

Morgan Redington and Eva Zurek*

Department of Chemistry, State University of New York at Buffalo, Buffalo, NY 14260-3000, USA

E-mail: ezurek@buffalo.edu

*To whom correspondence should be addressed

Abstract

High-temperature high-pressure superconducting hydrides are typically characterized by cage-like hydrogenic lattices filled with electropositive metal atoms. Here, density functional theory based evolutionary crystal structure searches find two phases that possess these geometric features and are related to the Type-II clathrate structure. In these $Fd\bar{3}m$ Li_2CaH_{16} and $R\bar{3}m$ Li_2CaH_{17} phases the calcium atom occupies the larger cage and the lithium atom the smaller one. The highest superconducting critical temperatures predicted within the isotropic Eliashberg formalism, 330 K at 350 GPa for $Fd\bar{3}m$ Li_2CaH_{16} and 370 K at 300 GPa for $R\bar{3}m$ Li_2CaH_{17}, suggest these structures are another example of hot superconducting hydrides. As pressure is lowered the cage-like lattices distort with the emergence of quasimolecular hydrogenic motifs; nonetheless Li_2CaH_{17} is predicted to be superconducting down to 160 GPa at 205 K.

Introduction

In 1968, Neil Ashcroft predicted that metallic hydrogen – the hypothetical ground state of the lightest element under pressure – could behave as a high-temperature superconductor.[1] The realization of this state has proven elusive, with the most recently estimated pressure needed being over 570 GPa[2]. Nearly four decades later Ashcroft described how the pressures required to metallize hydrogen could be decreased via addition of a second element that "chemically precompressed" the system.[3] As early as 2015, experimental studies supporting Ashcroft's prediction came to the fore. These included measurements of high superconducting critical temperatures (T_cs) in phases with unique stoichiometries, stable only under pressure, including H_3S (T_c = 203 K, 150 GPa),[4] LaH_{10} (T_c = 260 K, 200 GPa),[5,6] YH_9 (T_c = 262 K, 182 GPa),[7] YH_6 (T_c = 224 K, 166 GPa),[8] CaH_6 (T_c = 210-215 K, 160-172 GPa),[9–11] and CeH_9[12–14] (T_c = 100 K, 166 GPa). Recently, local magnetometry experiments on CeH_9, performed via nitrogen-vacancy centers embedded within the diamond anvil, provided evidence of the Meissner effect.[15]

The immense pressures required to stabilize the superconducting binary hydrides can only be reached in diamond anvil cells and come coupled with experimental intricacy and expense, making theoretical calculations an appealing method to both determine systems of interest and interpret experimental results.[16,17] Density functional theory (DFT) calculations have been found capable of predicting superconducting properties of conventional superconductors, and crystal structure prediction (CSP) techniques have been successful in uncovering promising synthetic targets (for unit cells that are not too complex).[18] The chemical space has been thoroughly scoured for fruitful high-temperature superconducting binary hydrides.[19–21] In contrast, ternary hydrides present relatively unexplored possibilities, however predictions for this class of hydrides are significantly more challenging.[22] The vast chemical space means that an increased number of stoichiometries must be considered for each elemental combination, with a more complex potential energy landscape that requires a greater number of structures be optimized in the CSP runs.[23] To overcome these challenges, machine learning potentials have been used to roughly explore the phase diagram prior to performing more costly DFT optimizations,[24] and high-throughput calculations have been em-

ployed to study elemental substitutions on previously-discovered superconducting templates.[25] The introduction of a third element could potentially be used to lower the stabilization pressure, such as in synthesized $LaBeH_8$ (T_c = 110 K, 80 GPa)[26] and predicted $BaSiH_8$ (T_c = 71 K, 3 GPa),[25] or increase the superconducting critical temperature as in the synthesized $(La,Ce)H_9$ (T_c = 148-178 K, 97-172 GPa)[27] and predicted Li_2ScH_{20} (T_c = 242 K, 300 GPa).[28] The former strategy is usually accomplished by using one electropositive element and one *p*-block element, whereas the latter strategy usually requires the combination of two electropositive elements. Recently, superconductivity in a quaternary hydride, $(La,Y,Ce)H_{10}$, has been reported with a maximum T_c of 190 K at 112 GPa.[29]

The hydrogenic lattices of the binary hydride superconductors of an electropositive element that have very high T_cs generally assume cage-like structures within which a metal atom is encapsulated. Several stoichiometries are well known. The MH_6 sodalite-like clathrate, first exemplified by CaH_6,[9–11] has a metal atom, M, centered in an H_{24} cage consisting of six square and eight hexagonal faces. The MH_9 structure, which surrounds the metal atom with an H_{29} cage of six irregular squares, six pentagons and six hexagons, is found in numerous rare-earth compounds including synthesized YH_9[7] and CeH_9.[12,13,15] Further increasing the hydrogen content, MH_{10} stoichiometries, where the metal atom sits within hydrogenic polyhedra of six squares and twelve hexagons, are perhaps the most well-known owing to the synthesis of the LaH_{10}[5,6] superhydride. The structure of the hydrogen lattice in these MH_{10} systems is known as "AST" in the clathrate and zeolite community.[30] More recently, larger hydride cages have been predicted to encapsulate rare earth metals. These include MH_{18} (M=Y, La, Ce, Ac, Th) stoichiometries with cubic ($Fmmm$ and $Fddd$) space groups, possessing H_{36} cages, with a maximum predicted T_c of 329 K at 350 GPa for CeH_{18}.[31] Can we draw inspiration from these systems and other occurring clathrates, specifically with phases that contain two electropositive elements?

Looking across the periodic table to other cage-forming elements we encounter silicon, which is able to form large polyhedral structures of sp^3 bonded Si atoms that are filled with metal atoms, characterizing the silicon clathrates (SiCL). Two of the most well studied SiCLs are the type-I $Pm\bar{3}m$

M_8Si_{24} (the Weaire-Phelan structure), which can be interpreted as two Si_{20} and 6 Si_{24} cages filled with a metal atom, and the type-II $Fd\bar{3}m$ $M_{x\leq 24}Si_{136}$ structure, which is made of 16 Si_{20} and 8 Si_{28} cages with a variable number of metal atoms that can be controlled by the synthesis conditions.[32–36] Several of the known silicon clathrates are superconductors, for example the type-I Ba_8Si_{46},[37] with an ambient pressure T_c of 8 K. Recent experiments report the synthesis of $(Ba/La/Eu)_4H_{23}$[38–40] high pressure hydrides in the type-I structure, with untested T_cs, and Lu_4H_{23},[41] with a T_c of 73 K at 218 GPa. Furthermore, predicted $Li_2(La/Y)H_{17}$[28] both match the type-II structure, with the highest T_c being 156 K at 160 GPa for Li_2LaH_{17}. These structure types have also been explored for Li_2NaH_{16}, Li_2NaH_{17}, and $LiNa_3H_{23}$,[42] predicting a maximum T_c of 340 K at 300 GPa for Li_2NaH_{17}. Prior to these structural correlations being drawn, a computational study predicted that when the MgH_{16}[43] structure was doped with Li, an $Fd\bar{3}m$ Li_2MgH_{16} "hot superconductor",[44] which differs from the type-II clathrate structure by a single unoccupied Wyckoff site (a clathrate atom at the (8a) 1/8, 1/8, 1/8 site), possessing a record calculated maximum T_c of 473 K at 250 GPa could be stabilized.[44]

Herein, through careful DFT calculations we investigated if a high-temperature superconductor analogous to Li_2MgH_{16},[44] but where Mg is replaced by Ca, could be stabilized under pressure. Because the type-I and type-II SiCL structures each possess two cages with distinct sizes, we hypothesized they would be particularly well suited templates for incorporating mixed metal atoms, and in our specific case lithium would fill the smaller cages and calcium the larger ones. Lithium is both electropositive, donating charge to the surrounding hydrogen lattice, and light, allowing for engaging in coupled high-frequency phonons with the hydrogen lattice. Furthermore, as several Ca hydrides are synthesized or predicted superconductors, we intended to improve upon their properties with the addition of Li. With these motivations, we performed CSP searches at megabar pressures for Li_2CaH_n ($n = 10 - 20$). Both stable and metastable phases were discovered, and their electronic structures were analyzed. Two dynamically stable metallic structures, one that is a distortion of the type-II SiCL, and one that can be derived from it, were found, and electron-phonon coupling calculations were performed to estimate their isotropic Eliashberg T_cs: 330 K at 350 GPa

for $Fd\bar{3}m$ Li_2CaH_{16}, and 205 K at 160 GPa or 370 K at 300 GPa for $R\bar{3}m$ Li_2CaH_{17}. This work extends the list of predicted "hot" superconducting ternary hydrides by two.

Methods

Exploratory crystal structure prediction (CSP) searches using the open-source XTALOPT[45,46] evolutionary algorithm (EA) 12th[47] release were performed to identify stable and metastable phases. EA runs were performed for the following stoichiometries: Li_2CaH_n (n=10-20) and Li_2Ca at 100, 200, and 300 GPa. The initial generation consisted of random symmetric structures created by the RANDSPG algorithm.[48] Duplicate structures were identified via the XTALCOMP algorithm for removal from the breeding pool.[49] The breeding operators employed and their relative probabilities were: (i) stripple (50%), (ii) permustrain (35%), and (iii) crossover (15%). The minimum number of generated structures was set to 1500. Each structure optimization consisted of four consecutive geometry optimizations, with each increasing in precision. The final geometry optimization step of the EA search employed a cutoff energy of 400 eV and a k-grid generated using the Γ-centered Monkhorst-Pack scheme,[50] with the number of divisions along each reciprocal lattice vector chosen such that the product of this number with the real lattice constant was 30 Å. After the EA searches concluded, the three most enthalpically favored unique structures at each stoichiometry and pressure were used for further analysis.

Precise geometry optimizations, electronic structure calculations, electron localization functions (ELF), Bader charges, and first principles molecular dynamics (FPMD) simulations were performed using DFT calculations with the PBE functional as implemented in the Vienna *Ab Initio* Simulation Package (VASP).[51,52] We employed a planewave basis set with an energy cutoff of 600 eV, along with PAW potentials[53] where the H $1s^1$, Li $1s^2 2s^1 2p^0$ and Ca $3p^6 4s^2 3d^{0.01}$ electrons were treated explicitly in all calculations. k-meshes were generated using the Γ-centered Monkhorst-Pack scheme,[50] and the number of divisions along each reciprocal lattice vector was chosen such that the product of this number with the real lattice constant was 50 Å. All FPMD

simulations were performed with a $2 \times 2 \times 2$ supercell, a single k-point at Γ, an NVT ensemble (constant number of particles, constant volume, constant temperature), Nosé-Hoover thermostat,[54] a 0.5 femtosecond timestep, and temperatures corresponding to the predicted T_cs. The crystal orbital Hamilton populations (COHPs) and the negative of the COHP integrated to the Fermi level (-iCOHP) were calculated using the LOBSTER package to analyze bonding.[55,56]

To determine if the predicted structures were dynamically stable, and obtain their zero-point energy, harmonic phonons were calculated using the supercell approach. In the supercell approach, Hellmann-Feynman forces were calculated from a supercell constructed by replicating the optimized structure wherein the atoms had been displaced, and dynamical matrices were computed using the PHONOPY code.[57] Quantum ESPRESSO (QE) was used to obtain the dynamical matrix and electron-phonon coupling (EPC) parameters.[58] H, Li, and Ca pseudopotentials obtained from the QE pseudopotential library were generated by the Vanderbilt ultrasoft method with a $1s^1$ configuration for H, a $1s^2 2s^1 2p^0$ configuration for Li, and a $3s^2 3p^6 4s^2 3d^0 4p^0$ configuration for Ca. The PBE functional was employed for all QE calculations. Plane-wave basis set cutoff energies were set to 70 Rydbergs (Ry) for all systems. The Methfessel-Paxton Brillouin-zone smearing of 0.015 Ry was applied.[59] The EPC parameter λ was calculated using Gaussian broadenings in increments of 0.005 Ry ranging from 0.005 to 0.050 Ry. A $15 \times 15 \times 15$ k-grid with a q-mesh of $5 \times 5 \times 5$ was employed for Li_2CaH_{17} at 300 GPa. Subsequent calculations on Li_2CaH_{17} utilized a q-mesh of $3 \times 3 \times 3$. This sparser q-mesh resulted in a deviation in λ of <2%, with a 20 K reduction in T_c, and an overall reduction in computational cost by 80%. This was determined to be sufficiently converged for prediction of EPC properties (Table S7). Therefore, a $15 \times 15 \times 15$ k-grid with a q-mesh of $3 \times 3 \times 3$ was utilized for Li_2CaH_{16}. For Li_2CaH_{17} the EPC appeared to be converged with these parameters at a broadening of 0.030 Ry, and Li_2CaH_{16} converged at a broadening of 0.050 Ry.

Critical temperature (T_c) values were obtained with a Coulomb repulsion parameter, μ^*, of 0.1 by the Allen-Dynes modified McMillan equation for strong coupling,

$$T_c = \frac{f_1 f_2 \omega_{\log}}{1.2} \exp\left[-\frac{1.04(1+\lambda)}{\lambda - \mu^*(1+0.62\lambda)}\right], \quad (1)$$

where $\omega_{\log}$ is the logarithmic average frequency and the f_1 and f_2 correction factors for strong coupling and shape dependence are functions of ω, λ, and μ^* (equaling unity for the weak coupling limit, see Ref.[60]). T_cs were also obtained by solving the isotropic Eliashberg equations[61] within the Fermi-surface-restricted (FSR) approximation numerically based on the spectral function, $\alpha^2F(\omega)$, obtained from the QE calculations. Isotropic solutions of T_c values in hydrides have been found to underestimate T_cs by $\leq 10\%$ compared to anisotropic solutions,[62–65] and a recent implementation has made it possible to compare the results of the full bandwidth (FBW) approach to those obtained with the FSR approach for hydrides.[66] The Matsubara frequency cutoff was set to a value of $20 \times \omega_2$, the root-mean-square phonon frequency, while the number of frequencies was allowed to vary up to 40,000.

Results and Discussion

Hydrogenic Motifs

Let us take a closer look at the predicted Li_2CaH_n structures, to better understand the peculiarities of their atomic configurations, and in particular the hydrogenic motifs that are so important for their superconducting properties. Based on the extensive work performed on binary high-pressure hydrides containing electropositive elements,[21,23] it is known that the presence of H^- and H_3^- anions is detrimental for superconductivity. When these molecules are present, the hydrides are metallized via pressure-induced broadening of the H^- and H_3^- bonding and anti-bonding bands, resulting in a low density of states (DOS) at the Fermi level (E_F) and no or low T_c[67,68]. Typically, compounds with H_2^- motifs are predicted to possess intermediate T_cs owing to the metallicity that stems from the partial filling of the antibonding H_2 σ_u^* orbitals, and a comparatively high DOS at E_F ($N(E_F)$). Expanding from molecules into extended hydrogenic lattices, a high $N(E_F)$ can be maintained. Compounds with cage-like lattices that enclathrate electropositive atoms are found to possess large values of λ, the electron-phonon coupling constant, leading to the highest computed and measured superconducting critical temperatures.[69]

Analysis of the structures found in our CSP searches reveals these same hydrogenic motifs, and illustrates how they vary as a function of hydrogen content and pressure (Table 1). The Li_2CaH_n $n = 10 - 13$ stoichiometries were typically characterized by H^- and bent, asymmetric H_3^- units, interspersed with H_2 molecules at all pressures investigated. The most stable $n = 14 - 15$ phases featured these same motifs at 100 and 200 GPa, however by 300 GPa incomplete clathrate cages began to emerge, suggesting that both the metal to hydrogen ratio and pressure are key for clathrate formation in the high-pressure hydrides. A clathrate cage is found within Li_2CaH_{16} at 300 GPa, but it dissociates to an incomplete clathrate at 200 GPa and further to a hydrogenic lattice containing discrete H_3^-, H_2 and H^- units by 100 GPa. The global minimum Li_2CaH_{17} phase possesses a clathrate structure at both 300 and 200 GPa, but dissociates to form H_2 and H^- by 100 GPa. Within Li_2CaH_{18} and Li_2CaH_{19} incomplete clathrates are present at 300 GPa, with H_2 units interspersed within the lattice for $n = 18$. At pressures of 100 and 200 GPa, these incomplete clathrates dissociate to form H_3^-, H_2 and H^-. Lastly, Li_2CaH_{20} possesses only H_2 units at 100, 200, and 300 GPa. Our observations are in-line with a chemical pressure analysis, which illustrates that clathrate formation in the high-pressure hydrides depends on the size-match between the metal cation and the hydrogenic cluster encapsulating it.[70] We postulated that the Li_2CaH_{16} and the Li_2CaH_{17} structures could be candidates for high-temperature, and perhaps "hot" superconductivity, given the proclivity of clathrate-structure-types for large EPC values.

Ternary Phase Diagrams

The most stable structures found in the CSP searches were employed to construct 3D convex hulls (Figures 1, S1-S3) at 100, 200, and 300 GPa at zero-temperature and within the clamped nuclei approximation. These plots are based upon the formation enthalpy as a function of the stoichiometry. By definition the convex hull connects phases whose enthalpies are lower than that of any other phase or linear combination of phases at a particular composition. Thus, the phases that lie on the hull are thermodynamically stable, whereas those that lie above it may be important local minima provided they are close to the hull, are dynamically stable, and are protected by sufficiently high

Table 1: Hydrogenic motifs for the most enthalpically favored phase of each stoichiometry at 100, 200, and 300 GPa.

Stoichiometry	**100 GPa**	**200 GPa**	**300 GPa**
Li_2CaH_{10}	H_3^-,H_2,H^-	H_2,H^-	H_3^-,H_2,H^-
Li_2CaH_{11}	H_2,H^-	H_2,H^-	H_2
Li_2CaH_{12}	H_2,H^-	H_2,H^-	H_3^-,H_2,H^-
Li_2CaH_{13}	H_2,H^-	H_2,H^-	H_2
Li_2CaH_{14}	H_2,H^-	H_2,H^-	Incomplete Clathrate
Li_2CaH_{15}	H_3^-,H_2,H^-	H_2,H^-	Incomplete Clathrate
Li_2CaH_{16}	H_3^-,H_2,H^-	Incomplete Clathrate	Clathrate
Li_2CaH_{17}	H_2,H^-	Clathrate	Clathrate
Li_2CaH_{18}	H_2,H^-	H_2,H^-	Incomplete Clathrate, H_2
Li_2CaH_{19}	H_3^-,H_2,H^-	H_3^-,H_2,H^-	Incomplete Clathrate
Li_2CaH_{20}	H_2	H_2	H_2

barriers. Therefore, it is often useful to plot the distance of a particular structure from the hull, to determine if it could be an important metastable phase. Because the compositions considered all possessed a 2:1 lithium to calcium ratio while the hydrogen content varied, 2D cuts of the generated convex hulls, corresponding to a plane of increasing H content from Li_2Ca at 100 GPa, or 2 Li + Ca at 200 and 300 GPa were also plotted (Figure S5, S6). At 300 GPa a Li_2CaH_{17} phase was predicted to be thermodynamically stable, while the structure closest to, but not on, the hull, Li_2CaH_{16}, lay 7 meV/atom above it (Table S2 and Figure 2). Notably, as discussed above, both of these possessed hydrogenic clathrate cages.

The zero-point-energy (ZPE) is often important in determining relative energy orderings for systems containing light elements, with the greatest potential influence on H-bearing phases, as they can have the highest frequency vibrations. For a given pressure the ZPE is affected by symmetry, with lower symmetry systems generally having larger ZPEs, and the nature of the hydrogenic motifs present within the crystal, with dihydrogen molecules having a larger ZPE than hydrogens within extended lattices such as clathrate cages. Indeed, it has been shown that the ZPE can affect the identity of the on-hull structures in high-pressure polyhydrides containing electropositive metal atoms.[71] Obtaining the ZPE necessitates performing phonon calculations, which allows for confirmation of dynamic stability, indicated by a lack of imaginary modes.

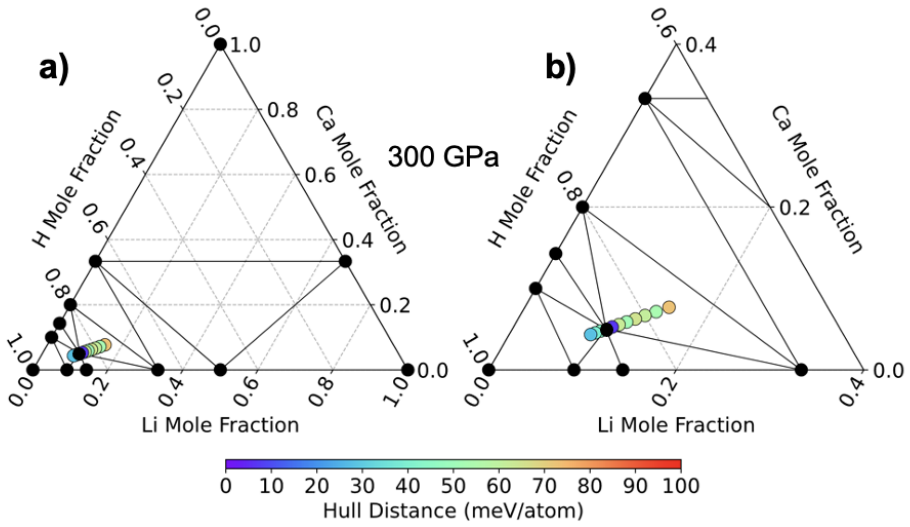

Figure 1: Distance of the most stable Li_2CaH_n (n=10-20) structures above the convex hull at 300 GPa. Panel (a) provides the full 3D convex hull at 300 GPa, while panel (b) focuses on hydrogen rich phases. Thermodynamically stable phases are shown in black, while metastable phases are colored based on their distance from the hull. The pure elemental phases of Ca,[72,73] Li,[74] and H,[75] optimized to the respective pressure, were used in constructing the convex hull. For binary phases the lithium hydrides LiH, LiH_2, and LiH_6,[67] LiH_9, and LiH_{10}[76] as well as the calcium hydrides CaH, CaH_2,[77] CaH_4, CaH_6,[11] CaH_9,[78] CaH_{12}, Ca_2H, and Ca_3H[79] were optimized to the respective pressure.

Phonon calculations, performed in the harmonic approximation, suggested that Li_2CaH_{17}, with a hydrogenic clathrate lattice, and Li_2CaH_n, n = (10,12,15,18-20), which did not feature clathrate structures, were dynamically stable at 300 GPa. Li_2CaH_{16}, on the other hand, possessed two modes with imaginary frequencies. These imaginary frequencies are related to the acoustic modes, with the majority of the atomic displacement being due to hydrogen. These frequencies were found to become real and positive by 350 GPa (Figure S21), indicating stabilization due to pressure. A first-principles molecular dynamics simulation at 330 K, however, showed that the hydrogenic lattice remained intact, with no molecular H units forming. This suggests one or more of the following: the phase is dynamically stable only at finite temperature; the system may be stabilized by the inclusion of anharmonicity or quantum effects; or the fineness of the grid needed to obtain real phonons is prohibitively computationally expensive. Due to the large size of the unit cell of Li_2CaH_{16}, and the associated computational expense, further calculations investigating this discrepancy and

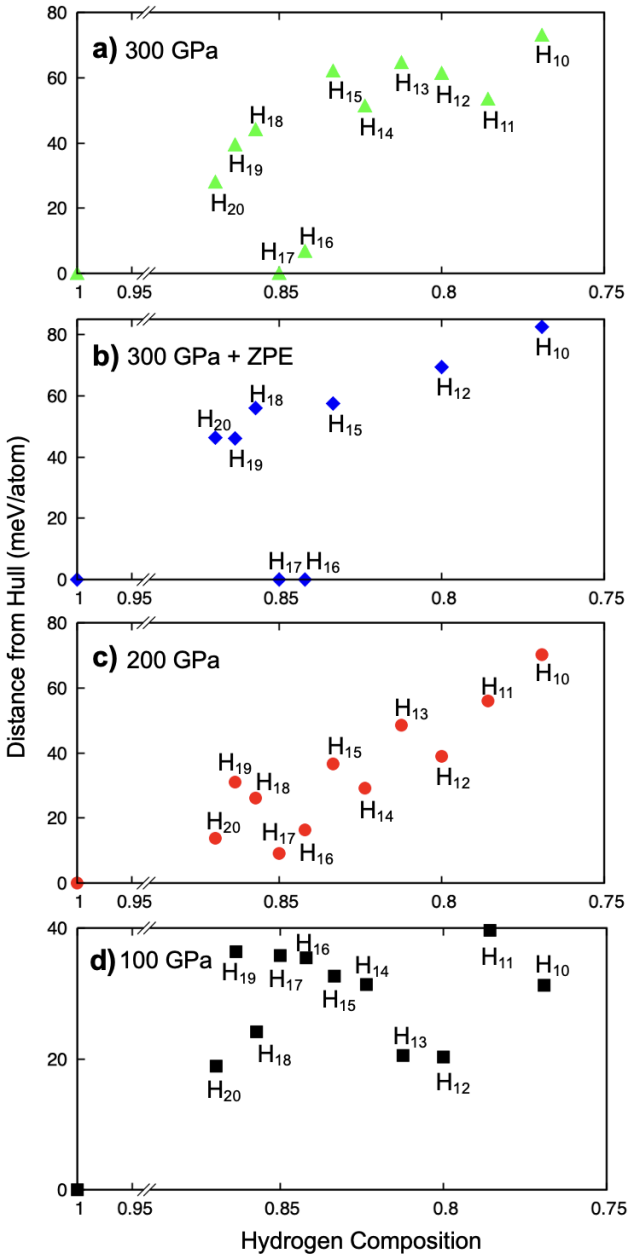

Figure 2: Distance of the most stable Li_2CaH_n (n=10-20) structures above the convex hull at (a,b) 300, (c) 200, and (d) 100 GPa. A two-dimensional cut of the three-dimensional Li-Ca-H convex hull corresponding to the plane between Li_2Ca (100 GPa) or 2Li + Ca (200 and 300 GPa) and elemental H is displayed. In panel (b) the distance is calculated using the zero-temperature enthalpies and the zero-point-energy (ZPE) corrections, and dynamically unstable phases are omitted. Li_2CaH_{16} is included, as it was show to be dynamically stable through first-principle molecular dynamics.

determining the lower boundary of dynamic stability were not performed, and the ZPE for this phase was estimated neglecting the imaginary modes. Figure 2(b) illustrates that inclusion of the

ZPE lowered the enthalpy of Li_2CaH_{16} so that it joined Li_2CaH_{17} on the 300 GPa hull, but the remaining non-clathrate structures became destabilized, lying at least 40 meV/atom above the hull.

Decreasing pressure moves all of the ternary hydrides progressively further from the hull. Li_2CaH_{16} shifts up to be 16 and 35 meV/atom above it, while Li_2CaH_{17} is calculated to be 9 and 36 meV/atom shy of thermodynamic stability at 200 and 100 GPa, respectively (Figures S1-S6). However, these compounds may still be promising at sub-300 GPa pressures, despite not laying on the hull, provided they are dynamically and thermally stable. Analysis of the zero-temperature DFT-computed enthalpies of the compounds contained in the Materials Project Database led to the estimate that ∼50% of known inorganic crystalline materials are metastable, with a median metastability energy of 15 meV/atom and a 90th percentile of 67 meV/atom.[80] For the specific case of high-pressure hydrides, whose synthesis at high-pressures in diamond anvil cells is often catalyzed by non-equilibrium processes such as thousands-of-Kelvin degree laser heating, numerous examples of synthesized DFT-metastable compounds are known. Some examples include Ca_2H_5,[77] which lays 20 meV/atom above the hull at 25 GPa, and various PH_n phases, which lay 30 meV/atom above the hull within the pressure range ∼80-225 GPa.[81–84]

Hydrogen Clathrate Structures

Plots of the enthalpy versus pressure of the low lying structures found in our CSP searches (Figures S7, S8) showed that $Fd\bar{3}m$ Li_2CaH_{16} became preferred (over other phases with this stoichiometry) above 270 GPa, while for Li_2CaH_{17} the $R\bar{3}m$ structure was the most stable above 140 GPa. From the other candidates found in our EA searches, these had the lowest enthalpies up to a maximum investigated pressure of 500 GPa. The propensity for high T_c in compounds with hydrogenic clathrate lattices, the observation that $Fd\bar{3}m$ Li_2CaH_{16} and $R\bar{3}m$ Li_2CaH_{17} both possessed such lattices with a high degree of symmetry, and the finding that both lay on the 300 GPa convex hull upon inclusion of the ZPE, prompted us to examine them in more detail.

$Fd\bar{3}m$ Li_2CaH_{16} is isotypic with previously predicted Li_2MgH_{16} and Li_2NaH_{16}.[42,44] In it, each Ca atom lies in a cage surrounded by four hexagons and twelve pentagons, made of 28 hydrogen

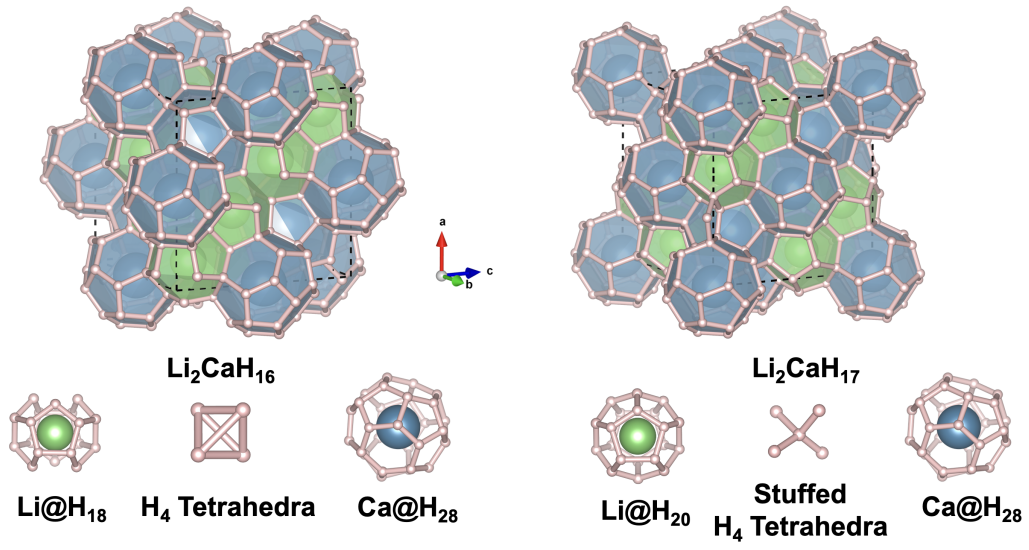

Figure 3: Crystal structures of predicted clathrate Li_2CaH_n structures. Cubic $Fd\bar{3}m$ Li_2CaH_{16} has $Li@H_{18}$ and $Ca@H_{28}$ cages, with H_4 tetrahedra. Trigonal $R\bar{3}m$ Li_2CaH_{17} (structure shown using cubic representation) has $Li@H_{20}$ and $Ca@H_{28}$ cages, with hydrogen stuffed H_4 tetrahedra. Calcium atoms are colored blue, lithium atoms are colored green, and hydrogen atoms are colored pink. Dashed lines represent unit cells, while the solid lines between hydrogens indicate weak bonds. Solid lines displayed for the unstuffed H_4 tetrahedra serve as a visual aid, and are not indicative of bonding.

atoms, and each Li atom is enclathrated in an 18 atom hydrogen cage with four hexagons and five pentagons. The size of the cages around each metal atom are commensurate with their radii, with Ca nestled in the larger cage and lithium sitting in the smaller cage, as illustrated in Figure 3. At 350 GPa these polygons are highly regular, with H-H bond lengths of 1.05, 1.08, and 1.12 Å. This $Fd\bar{3}m$ symmetry lattice is markedly similar to the type-II SiCL structure, differing by a single Wyckoff position. While the clearest hydrogen motifs in $Fd\bar{3}m$ Li_2CaH_{16} are the H_{18} and H_{28} cages, we can also view the structure as possessing eight H_4 tetrahedra in the conventional cell ($Z = 8$), corresponding to one H_4 tetrahedra per formula unit. These H_4 tetrahedra are centered around the unfilled Wyckoff position, a clathrate atom at the (8a) 1/8, 1/8, 1/8 site, that if filled would make them isotypic to the type-II SiCL structure.

In $R\bar{3}m$ Li_2CaH_{17}, also shown in Figure 3, each Ca atom is surrounded by four hexagons and twelve pentagons, and each Li atom is once again found in the smaller cage, surrounded by eleven

pentagons. The additional hydrogen atom in $R\bar{3}m$ Li_2CaH_{17} renders the $R\bar{3}m$ phase nearly isostructural with the type-II SiCLs. In comparison with $Fd\bar{3}m$ Li_2CaH_{16}, $R\bar{3}m$ Li_2CaH_{17} possesses H_4 tetrahedra "stuffed" with the extra hydrogen atom, which assists in completing the cage around the Li ions. The stuffed hydrogen atom may stabilize this structure by balancing the chemical pressure interactions within the lattice, as has been observed in the H-stuffed H_4 tetrahedra of LaH_{10},[70] or by allowing the structure to distort more readily. These distortions can be seen with the reduced symmetry of the faces comprising the polygons that make up the clathrate; each pentagon has H-H bond lengths between 1.08 and 1.14 Å, while each hexagon has H-H bond lengths between 1.02 and 1.14 Å at 300 GPa. Investigation of the $R\bar{3}m$ Li_2CaH_{17} phase shows that these bonds become less uniform as pressure decreases. The $R\bar{3}m$ phase was determined to be dynamically stable down to 160 GPa, however the full clathrate structure does not persist to this pressure, due to the H-H bond lengths increasing (e.g. see ELF plot in Figure S20).

$R\bar{3}m$ Li_2CaH_{17} was not anticipated to be the most stable spacegroup for this stoichiometry. Previous studies have predicted an $Fd\bar{3}m$ M_3H_{17} phase, where M is a metal atom, in compounds such as Li_2(Sc/La/Y/Na)H_{17}.[28,42] These $Fd\bar{3}m$ symmetry M_3H_{17} phases are isostructural with the type-II SiCL, while the $R\bar{3}m$ Li_2CaH_{17} phase can be seen as a distortion of this structure. The external pressure, internal (or chemical pressure) and the number of valence electrons that are transferred from the metal atoms to the hydrogen cage, and potential metal-hydrogen interactions may be important factors driving this distortion. The external pressure most directly affects the pV (pressure-volume) term to the enthalpy, often favoring the formation of closed packed structures at higher pressures. The chemical pressure is related to the ionic radius of the metal atom and how it fits into the cage, with ions that are too-small or too-large resulting in distorted lattices.[70] The number of valence electrons that are donated from the electropositive element to the hydrogenic lattice can influence the types of hydrogenic motifs that are present,[11] and the resulting H-H distances, which are also influenced by interactions such as Ca d $\rightarrow$ H_2 σ^* backbonding.[77] To confirm that the $R\bar{3}m$ phase is indeed favored over $Fd\bar{3}m$, the cubic structure was built and optimized. Comparison of the 300 GPa enthalpies revealed that the $R\bar{3}m$ phase possessed a lower internal energy, U, but a higher pV term.

The bonds in the $R\bar{3}m$ phase are more distorted than the highly ordered $Fd\bar{3}m$ phase, and these distortions likely contribute to the enthalpic favorability of the $R\bar{3}m$ structure for the metal atoms studied here. Furthermore, the $Fd\bar{3}m$ phase of Li_2CaH_{17} was determined to be both dynamically unstable at 300 GPa, and enthalpically disfavored over the pressure range of 100-500 GPa, so it was therefore not considered for additional calculations.

A similar phenomenon of competing phases has recently been investigated in the LaH_{10} system.[85] While DFT calculations with classical nuclei and neglecting anharmonic effects predicted that an $Fm\bar{3}m$ phase becomes unstable with respect to distorted phases including rhombohedral $R\bar{3}m$ LaH_{10} below 230 GPa, the inclusion of quantum fluctuations resulted in the dynamic stability of the $Fm\bar{3}m$ phase across a wide pressure regime. Moreover, the competing phases all converged to $Fm\bar{3}m$ LaH_{10} when quantum fluctuations were applied in the structural relaxation. While it is possible that quantum fluctuations could stabilize $Fd\bar{3}m$ Li_2CaH_{17} over the $R\bar{3}m$ phase, these calculations were not performed for several reasons. First, an increased measure of non-uniformity among the H-H bonds that make up the clathrate faces is observed for FPMD simulations at 370 K, which is in alignment with the $R\bar{3}m$ phase, but not the highly symmetric $Fd\bar{3}m$ phase. Since the thermal energy provided by the thermostat is far in excess of the stabilization energy due to quantum fluctuations in hydrides, this distortion would be expected if the cubic structure was preferred. Moreover, at no point over the pressure regime did the $Fd\bar{3}m$ phase become thermodynamically preferred over the $R\bar{3}m$ phase, in contrast to the behavior observed for LaH_{10}. Finally, the computational expense required was seen as overly prohibitive, though recently developed machine-learning approaches may make these types of calculations possible in the future.[86] Compared to molecular H-H bonds at the same pressure, the H-H bond lengths in both $R\bar{3}m$ Li_2CaH_{17} and $Fd\bar{3}m$ Li_2CaH_{16} are longer (Table 2). Bader analysis showed that the caged Li and Ca atoms donate charge to the nearby hydrogen atoms, which may covalently bond with one another. For $R\bar{3}m$ Li_2CaH_{17} at 160 GPa, each H atom gains on average $0.16e^-$, with Ca losing $1.05e^-$ and Li donating a smaller amount of charge, $0.84e^-$. When the pressure is increased to 300 GPa, each H atom in $R\bar{3}m$ Li_2CaH_{17} gains on average $0.15e^-$, while Ca loses $0.89e^-$ and Li donates $0.80e^-$. Thus, increasing pressure appears to

even out the amount of charge transferred from both the formally divalent and monovalent metal atoms, perhaps because a shorter distance between the hydrogen atom and calcium can enhance the amount of backdonation between the occupied antibonding hydrogen-lattice states and the Ca d orbitals, as previously found within compressed CaH_4 [77] and Ca-S-H ternary hydrides.[87] The Bader charges calculated for $Fd\bar{3}m$ Li_2CaH_{16} at 350 GPa are similar, with H gaining $0.15e^-$ on average, and Ca and Li donating $0.90e^-$ and $0.78e^-$, respectively.

Table 2: Distances and -iCOHPs for select H-H atom pairs in $Fd\bar{3}m$ Li_2CaH_{16}, $R\bar{3}m$ Li_2CaH_{17}, $C2/c$ H_2, and $Im\bar{3}m$ CaH_6. The "Edges" column specifies how many bonds of that length make up the edges of hexagons, pentagons, and/or squares that comprise the clathrate faces.

System	Pressure (GPa)	$r_{H\text{-}H}$ (Å)	-iCOHP (eV/bond)†	Edges
$Fd\bar{3}m$ Li_2CaH_{16}	350	1.05	2.12 (2.04)	2x ⬠
		1.08	1.67 (1.98)	6x ⬡, 2x ⬠
		1.12	1.44 (1.60)	1x ⬠
$C2/c$ H_2	350	0.75	6.37	
		1.14	1.16	
$R\bar{3}m$ Li_2CaH_{17}	300	1.00	2.60 (2.45)	1x ⬠
		1.03	2.09 (2.46)	2x ⬡, 1x ⬠
		1.08	2.32 (2.00)	2x ⬠
		1.09	1.85 (1.83)	2x ⬠
		1.13	1.23 (1.65)	6x ⬡
		1.14	1.46 (1.54)	4x ⬡, 2x ⬠
$C2/c$ H_2	300	0.75	6.35	
		1.14	1.13	
$Im\bar{3}m$ CaH_6	300	1.15	1.33	6x ⬡, 4x □

† The -iCOHP values for a hypothetical lattice of hydrogen where no Li or Ca is present, but the H positions are unchanged are provided in parentheses.

To further investigate the bonding within the hydrogenic lattice, the negative of the crystal overlap Hamiltonian population, integrated to the Fermi level (-iCOHP), was calculated for $Fd\bar{3}m$ Li_2CaH_{16} and $R\bar{3}m$ Li_2CaH_{17} at 350 and 300 GPa, respectively, and compared to the -iCOHP for the $C2/c$ phase of molecular hydrogen at the same pressure (Table 2). Unsurprisingly, the intermolecular -iCOHP for $C2/c$ H_2 was significantly stronger than that obtained for the shortest distance in the ternary hydrides (6.37 vs. 2.12 eV/bond, and 6.35 vs. 2.60 eV/bond, respectively). Interestingly, though the shortest intramolecular distances within $C2/c$ H_2 were nearly identical to the longest

H-H bonds in $Fd\bar{3}m$ Li_2CaH_{16} and $R\bar{3}m$ Li_2CaH_{17}, the -iCOHPs calculated for these atom pairs in the clathrate cages were somewhat stronger (1.16 vs. 1.44 eV/bond, and 1.13 vs. 1.46 eV/bond, respectively). We can compare the -iCOHPs of the $Li_2CaH_{16/17}$ phases with those computed for the compressed calcium polyhydrides, in particular $Im\bar{3}m$ CaH_6, a sodalite-like structure with a hydrogen cage. At 300 GPa, the bond measuring 1.15 Å in $Im\bar{3}m$ CaH_6 has an -iCOHP value of 1.33 eV/bond, making it slightly weaker than the 1.14 Å H-H bond in $R\bar{3}m$ Li_2CaH_{17} at 300 GPa (1.46 eV/bond). Removing the alkali and alkaline earth metal atoms from the lattice, but without any further relaxation, yields a different set of -iCOHP values, illustrating how these electropositive elements affect the bonding in the hydrogen lattice. Though in some cases the interactions are strengthened and in other times they are weakened by the presence of the metal atoms, overall the -iCOHPs computed for the empty cages become more equalized with a somewhat smaller spread.

Electronic Structure and Superconductivity

$Fd\bar{3}m$ Li_2CaH_{16} and $R\bar{3}m$ Li_2CaH_{17} are calculated to have a high $N(E_F)$ (Figure 4), primarily of hydrogen *s* character, boding well for superconductivity. The contribution of the calcium states to $N(E_F)$ is intermediate, while the contribution of the lithium states is minimal. Therefore, the DOS plots are consistent with a Li^+ cation, and a not-fully-ionized calcium, resulting from the back-donation of charge from the hydrogenic lattice to the Ca d orbitals, as supported by the large amount of Ca d states at E_F. In $Fd\bar{3}m$ Li_2CaH_{16} at 350 GPa and $R\bar{3}m$ Li_2CaH_{17} at 300 GPa E_F lies just below a peak in the DOS, suggesting that further electron doping (*e.g.* by replacing Li via a divalent metal atom with a similar ionic radius, or Ca by a trivalent metal atom) could potentially enhance T_c. Such peaks in the DOS have previously been reported in $Fd\bar{3}m$ symmetry Li_2NaH_{17} (just above E_F) and Li_2YH_{17} (just below E_F) at 300 GPa.[28,42] Assuming a full transfer of electrons from the electropositive element to the hydrogenic lattice yields three-donated-electrons in Li_2NaH_{17} and four-donated-electrons in Li_2CaH_{17}. In both of these systems E_F sits below the peak in the DOS, so more electrons must be added. However, in Li_2YH_{17}, with five-donated-electrons, E_F lies

just above the peak. Thus, the optimal number of electron required to maximize T_c is between four and five. We find that adding an additional 0.38 e^- per FU (formula unit) (~4 e^-/10 FU) to Li_2CaH_{16} at 350 GPa and an additional 0.40 e^- per FU (4 e^-/ 10 FU) to Li_2CaH_{17} at 300 GPa would place E_F on that peak. Therefore, a quaternary compound with an approximate $Li_2Ca_{0.6}M_{0.4}H_{16/17}$ stoichiometry, where M is a trivalent metal ion such as Sc, Y, or La may potentially result in a higher T_c than those calculated here, provided the structure is dynamically stable.

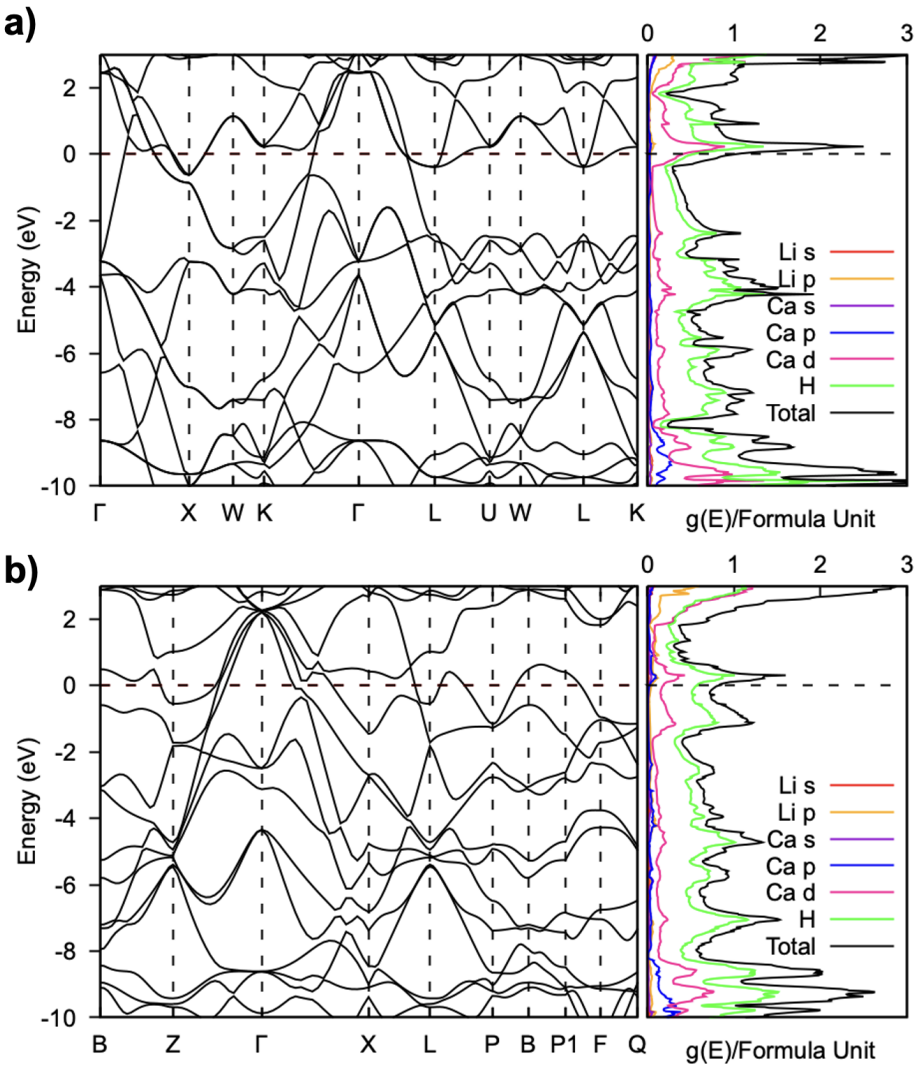

Figure 4: The electronic band structure and projected density of states, with the Fermi energy set to 0 eV for (a) $Fd\bar{3}m$ Li_2CaH_{16} at 350 GPa and (b) $R\bar{3}m$ Li_2CaH_{17} at 300 GPa.

The descriptors for high-T_c superconductivity – λ and the logarithmic average phonon fre-

quency, $\omega_{\log}$ – were computed for these two phases at pressures where they were dynamically stable (Table 3). The λ parameter provides the strength of the electron-phonon coupling in conventional superconductors and falls in the exponential in the semi-empirical Allen-Dynes modified McMillan equation often used to estimate T_c (Equation 1). The $\omega_{\log}$ parameter lies in the pre-factor of Equation 1. A short overview of the various methods that are commonly used to estimate T_c can be found in Ref.[23]

For $Fd\bar{3}m$ Li_2CaH_{16}, imaginary modes were absent only at 350 GPa, where this phase possessed the largest $N(E_F)$ that we computed. The large λ of 2.58 necessitated that the Eliashberg equations be solved numerically, and using a value of 0.1 for the Coulomb shielding parameter, μ^*, we obtained a T_c of 330 K for $Fd\bar{3}m$ Li_2CaH_{16} at this pressure. Though this predicted T_c is over 100 K lower than that computed for the isotypic Li_2MgH_{16} at 250 GPa,[44] it surpasses room temperature, rendering Li_2CaH_{16} a "hot" superconductor. Its phonon band structure, phonon projected densities of states and Eliashberg spectral function are shown in Figure 5(a). Because of the mass differences between the three atom types, the phonons can be well separated into regions where the contributions from a particular atom are dominant. Therefore, the total EPC could be partitioned into contributions originating from vibrations in the low-frequency regime, projected mostly onto the calcium atoms (15%), followed by a lithium-dominant region (9%), then by the mainly hydrogenic modes above 750 cm^{-1} (76%). No high-frequency modes indicative of the presence of molecular hydrogen units were observed, with the highest vibrational frequency being 2385 cm^{-1}, in-line with the previously computed value of 2400 cm^{-1} for Li_2MgH_{16} at 300 GPa.[44] The much higher λ of Li_2MgH_{16} at 300 GPa compared to that of Li_2CaH_{16} at 350 GPa (3.35 vs. 2.58) is likely in part due to the lower pressure at which it could be stabilized, as λ was shown to decrease with increasing pressure.[44] The larger λ and lighter mass of Mg as compared to Ca are both factors that result in the higher T_c of Li_2MgH_{16}. Another compound that resembled $Fd\bar{3}m$ Li_2CaH_{16}, $Pm\bar{3}n$ $LiNa_3H_{23}$with a type-I SiCL structure, possessed a very similar $N(E_F)$, λ and therefore a very similar T_c of 310 K at 350 GPa was predicted.[42]

Let us now turn to $R\bar{3}m$ Li_2CaH_{17}, whose EPC was well above the threshold requiring the

Table 3: Superconducting parameters for $Fd\bar{3}m$ Li_2CaH_{16} and $R\bar{3}m$ Li_2CaH_{17}. T_c was calculated with $\mu^* = 0.1$, by employing both the McMillan Allen-Dynes-modified (MAD) equation (Equation 1)[60] and numerically solving the isotropic Eliashberg (El) equations. The density of states at the Fermi level, $N(E_F)$, is provided in units of states/eV/formula unit, and S is the superconducting figure of merit.[88]

System	Pressure (GPa)	λ	ω_{log}(K)	$N(E_F)$	T_c^{MAD} (K)	T_c^{El} (K)	S
$Fd\bar{3}m$ Li_2CaH_{16}	350	2.58	1123	1.23	272	330	0.94
$R\bar{3}m$ Li_2CaH_{17}	300	2.56	1314	0.99	283	370	1.22
$R\bar{3}m$ Li_2CaH_{17}	220	3.42	922	0.84	286	317	1.42
$R\bar{3}m$ Li_2CaH_{17}	160	1.72	1194	0.74	179	205	1.24

use of the Eliashberg formalism in the studied pressure range: 2.56 at 300 GPa and 1.72 at 160 GPa. At 300 GPa the predicted T_c, 370 K, was near the boiling point of water on Earth's surface, rendering this another example of a "hot" superconductor. This critical temperature, while lower than that predicted for $Fd\bar{3}m$ Li_2MgH_{16}, has greatly improved upon the T_c of CaH_6. At this pressure vibrations that fell in the primarily Ca-based low frequency region contributed 15% to the total EPC, whereas Li-dominant vibrations contributed 4%, and primarily H vibrations contributed 81%. The superconducting properties of $R\bar{3}m$ Li_2CaH_{17} can be compared directly to Li_2ScH_{17}, Li_2YH_{17}, Li_2LaH_{17}, and Li_2NaH_{17}, hydride superconductors with similar structures[28,42] (Table S8). Li_2CaH_{17} and Li_2NaH_{17} not only stand out as being better metals than Li_2ScH_{17}, Li_2YH_{17}, and Li_2LaH_{17}, but also have much larger EPCs, leading to much higher predicted T_cs. Calculations performed with the Allen-Dynes modified McMillan equation for strong coupling (Equation 1) yielded lower estimates of the T_c.

Both the $N(E_F)$ and the T_c decreased with decreasing pressure for Li_2CaH_{17}, although λ was highest at 220 GPa, where ω_{log} was lowest. Analysis of the structure and the ELF (Figure S19) revealed that the hydrogen clathrate is beginning to break apart into molecular units at this pressure, leading to the large increase in λ caused by the structural instability. However, these molecular units reduce T_c in-line with previously observed trends.[23] The formation of molecular units becomes more pronounced as pressure decreases, and by 160 GPa 50% of the hydrogen atoms constitute H_2 or H_3^- molecules, with the other half of the hydrogens forming 9-membered rings, decreasing

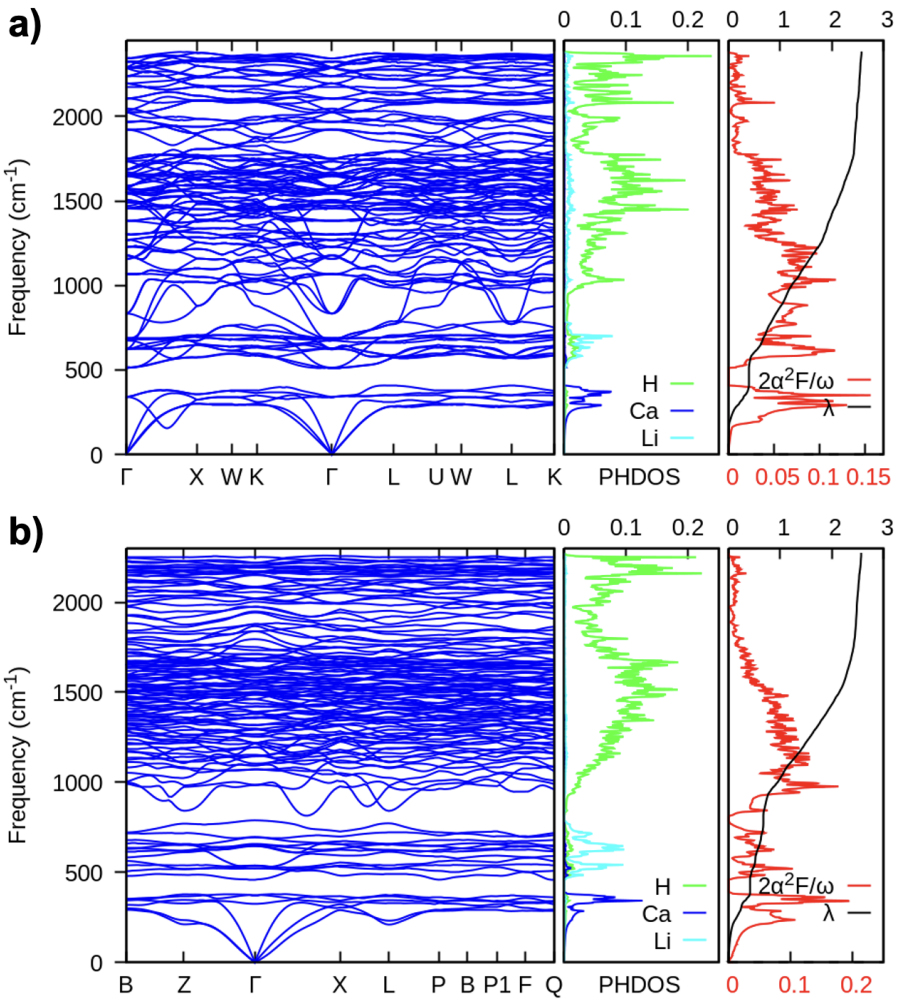

Figure 5: Phonon dispersion curves, projected phonon density of states (PHDOS), Eliashberg spectral function scaled by the frequency ($2\alpha^2F/\omega$), and the integrated electron-phonon coupling constant (λ). (a) Properties for $Fd\bar{3}m$ Li_2CaH_{16} at 350 GPa. (b) Properties for $R\bar{3}m$ Li_2CaH_{17} at 300 GPa.

λ and the calculated T_c even further. The T_c for $R\bar{3}m$ Li_2CaH_{17} at 160 GPa is calculated to be 205 K, surprisingly similar to that of CaH_6 (T_c = 210-215 K, 160-172 GPa).[9–11] At 160 GPa, the limit of dynamical stability for $R\bar{3}m$ Li_2CaH_{17} (Figure S23), its superconducting figure of merit,[88] $S = 1.24$, is markedly similar to that of $Im\bar{3}m$ H_3S at 150 GPa, 1.31, and somewhat larger than that of $Fd\bar{3}m$ Li_2LaH_{17} at 160 GPa, 0.95.[4,28] The highest phonon modes for $R\bar{3}m$ Li_2CaH_{17} are 2275 cm^{-1} at 300 GPa and 2190 cm^{-1} at 160 GPa. These modes can be compared to the highest

phonon modes for atomic metallic hydrogen at 500 GPa being approximately 2600 cm^{-1},[89] with those of LaH_{10} being 2300 cm^{-1} at 300 GPa[5,6] and for CaH_6 being near 2000 cm^{-1} at 150 GPa.[11]

Conclusions

Previous theoretical calculations have predicted that "hot superconductors", compounds that are superconducting at room temperature and above, may be stabilized under extreme pressures.[31,42,44] Interest in these materials stems from the fact that quantum behavior at atmospheric pressures is typically only observed at low temperatures. Herein, crystal structure prediction searches combined with density functional theory calculations predict two new hot superconductors, with critical temperatures, T_cs, as high as 330 K at 350 GPa for $Fd\bar{3}m$ Li_2CaH_{16} and 370 K at 300 GPa for $R\bar{3}m$ Li_2CaH_{17}. These ternary hydride phases are predicted to lie on the 300 GPa convex hull (when zero-point-energy effects are included). Li_2CaH_{17} was found to be dynamically stable down to 160 GPa in the harmonic approximation, where its T_c was predicted to be similar to previously-synthesized H_3S[4] and CaH_6.[9–11]

The structures of $Fd\bar{3}m$ Li_2CaH_{16} and $R\bar{3}m$ Li_2CaH_{17} can both be described as clathrate-like hydrogenic lattices where the heavier calcium cation occupies the larger H_{28} cages, and the smaller lithium cation is situated within H_{18} or H_{20} encapsulations. Both of these phases are related to the Type-II clathrate structure with Li_2CaH_{17} being a rhombohedral distortion of the $Fd\bar{3}m$ symmetry lattices found in the silicon variants, and $Fd\bar{3}m$ Li_2CaH_{16} being derived from the ideal Type-II clathrate structure via removal of a single hydrogen atom. We postulate that the T_c in these ternary hydrides could be enhanced by tuning the average valence of the enclathrated electropositive metal atoms so that the Fermi level sits on the peak in the densities of states, resulting in compositions such as $Li_2Ca_{0.6}M_{0.4}H_{16/17}$, where M is a trivalent metal ion.

Acknowledgements

Funding for this research was provided by the NSF award DMR-2136038 and the U.S. Department of Energy, National Nuclear Security Administration, through the Chicago-DOE Alliance Center (CDAC) under Cooperative Agreement DE-NA0003975. E.Z. acknowledges the U.S. Department of Energy, Office of Science, Fusion Energy Sciences funding the award entitled High Energy Density Quantum Matter under Award No. DE-SC0020340. Calculations were performed at the Center for Computational Research at SUNY Buffalo (https://hdl.handle.net/10477/79221). M.R. would like to thank Dr. Francesco Belli for discussions regarding quantum fluctuations and electron-phonon coupling.

Supporting Information Available

The Supporting Information is available free of charge on the publication website, `http://pubs.acs.org/`. It includes the space group at various pressures, distance above the convex hull, relative enthalpies, equation of states, electronic band structures and densities of states, electron localization functions, Bader charges, phonon density of states, computational parameters in EPC calculations, plots of first-principle molecular dynamic simulation results, superconducting properties of selected phases, and structural parameters. The optimized structures were deposited in as *cif* files in the Theoretical Crystallography Open Database (TCOD IDs: 30000120-30000153).

Notes

The authors declare no competing financial interest.

References

(1) Ashcroft, N. W. Metallic Hydrogen: A High-Temperature Superconductor? *Phys. Rev. Lett.* **1968**, *21*, 1748–1748

(2) Monacelli, L.; Casula, M.; Nakano, K.; Sorella, S.; Mauri, F. Quantum phase diagram of high-pressure hydrogen. *Nat. Phys.* **2023**, *19*, 845–850

(3) Ashcroft, N. W. Hydrogen Dominant Metallic Alloys: High Temperature Superconductors? *Phys. Rev. Lett.* **2004**, *92*, 187002

(4) Drozdov, A. P.; Eremets, M. I.; Troyan, I. A.; Ksenofontov, V.; Shylin, S. I. Conventional superconductivity at 203 kelvin at high pressures in the sulfur hydride system. *Nature* **2015**, *525*, 73–76

(5) Somayazulu, M.; Ahart, M.; Mishra, A. K.; Geballe, Z. M.; Baldini, M.; Meng, Y.; Struzhkin, V. V.; Hemley, R. J. Evidence for Superconductivity above 260 K in Lanthanum Superhydride at Megabar Pressures. *Phys. Rev. Lett.* **2019**, *122*, 027001

(6) Drozdov, A. P.; Kong, P. P.; Minkov, V. S.; Besedin, S. P.; Kuzovnikov, M. A.; Mozaffari, S.; Balicas, L.; Balakirev, F. F.; Graf, D. E.; Prakapenka, V. B.; Greenberg, E.; Knyazev, D. A.; Tkacz, M.; Eremets, M. I. Superconductivity at 250 K in lanthanum hydride under high pressures. *Nature* **2019**, *569*, 528–531

(7) Kong, P. P.; Minkov, V. S.; Kuzovnikov, M. A.; Drozdov, A. P.; Besedin, S. P.; Mozaffari, S.; Balicas, L.; Balakirev, F. F.; Prakapenka, V. B.; Chariton, S.; Knyazev, D. A.; Greenberg, E.; Eremets, M. I. Superconductivity up to 243 K in the yttrium-hydrogen system under high pressure. *Nat. Commun.* **2021**, *12*, 5075

(8) Troyan, I. A. et al. Anomalous High-Temperature Superconductivity in YH_6. *Adv. Mater.* **2021**, *33*, 2006832

(9) Ma, L.; Wang, K.; Xie, Y.; Yang, X.; Wang, Y.; Zhou, M.; Liu, H.; Yu, X.; Zhao, Y.; Wang, H.; Liu, G.; Ma, Y. High-Temperature Superconducting Phase in Clathrate Calcium Hydride CaH_6 up to 215 K at a Pressure of 172 GPa. *Phys. Rev. Lett.* **2022**, *128*, 167001

(10) Li, Z. W. et al. Superconductivity above 200 K discovered in superhydrides of calcium. *Nat. Commun.* **2022**, *13*, 2863

(11) Wang, H.; Tse, J. S.; Tanaka, K.; Iitaka, T.; Ma, Y. Superconductive Sodalite-like Clathrate Calcium Hydride at High pressures. *Proc. Natl. Acad. Sci. U.S.A.* **2012**, *109*, 6463–6466

(12) Salke, N. P.; Mahdi Davari Esfahani, M.; Zhang, Y.; Kruglov, I. A.; Zhou, J.; Wang, Y.; Greenberg, E.; Prakapenka, V. B.; Liu, J.; Oganov, A. R.; Lin, J.-F. Synthesis of Clathrate Cerium Superhydride CeH_9 at 80-100 GPa with Atomic Hydrogen Sublattice. *Nat. Commun.* **2019**, *10*, 4453–4453

(13) Li, X.; Huang, X.; Duan, D.; Pickard, C. J.; Zhou, D.; Xie, H.; Zhuang, Q.; Huang, Y.; Zhou, Q.; Liu, B.; Cui, T. Polyhydride CeH_9 with an Atomic-Like Hydrogen Clathrate Structure. *Nat. Commun.* **2019**, *10*, 3461–3461

(14) Peng, F.; Sun, Y.; Pickard, C. J.; Needs, R. J.; Wu, Q.; Ma, Y. Hydrogen Clathrate Structures in Rare Earth Hydrides at High Pressures: Possible Route to Room-Temperature Superconductivity. *Phys. Rev. Lett.* **2017**, *119*, 107001–107001

(15) Bhattacharyya, P. et al. Imaging the Meissner effect in hydride superconductors using quantum sensors. *Nature* **2024**, *627*, 73–79

(16) Zurek, E.; Grochala, W. Predicting Crystal Structures and Properties of Matter Under Extreme Conditions via Quantum Mechanics: the Pressure is On. *Phys. Chem. Chem. Phys.* **2015**, *17*, 2917–2934

(17) Miao, M.; Sun, Y.; Zurek, E.; Lin, H. Chemistry under high pressure. *Nat. Rev. Chem.* **2020**, *4*, 508–527

(18) Flores-Livas, J. A.; Boeri, L.; Sanna, A.; Profeta, G.; Arita, R.; Eremets, M. A perspective on conventional high-temperature superconductors at high pressure: Methods and materials. *Phys. Rep.* **2020**, *856*, 1–78

(19) Bi, T.; Zarifi, N.; Terpstra, T.; Zurek, E. *Reference Module in Chemistry, Molecular Sciences and Chemical Engineering*; Elsevier, 2019; pp 1–36

(20) Wang, H.; Li, X.; Gao, G.; Li, Y.; Ma, Y. Hydrogen-Rich Superconductors at High Pressures. *Wiley Interdiscip. Rev. Comput. Mol. Sci.* **2017**, *8*, 1–13

(21) Zurek, E.; Bi, T. High-Temperature Superconductivity in Alkaline and Rare Earth Polyhydrides at High Pressure: A Theoretical Perspective. *J. Chem. Phys.* **2019**, *150*, 050901–050901

(22) Lilia, B. et al. The 2021 room-temperature superconductivity roadmap. *J. Phys. Condens. Matter* **2022**, *34*, 183002

(23) Hilleke, K. P.; Zurek, E. Tuning chemical precompression: Theoretical design and crystal chemistry of novel hydrides in the quest for warm and light superconductivity at ambient pressures. *J. Appl. Phys.* **2022**, *131*, 070901

(24) Ferreira, P. P.; Conway, L. J.; Cucciari, A.; Di Cataldo, S.; Giannessi, F.; Kogler, E.; Eleno, L. T. F.; Pickard, C. J.; Heil, C.; Boeri, L. Search for ambient superconductivity in the Lu-N-H system. *Nat. Commun.* **2023**, *14*, 5367

(25) Lucrezi, R.; Di Cataldo, S.; von der Linden, W.; Boeri, L.; Heil, C. In-silico synthesis of lowest-pressure high-Tc ternary superhydrides. *Npj Comput. Mater.* **2022**, *8*, 119

(26) Song, Y.; Bi, J.; Nakamoto, Y.; Shimizu, K.; Liu, H.; Zou, B.; Liu, G.; Wang, H.; Ma, Y. Stoichiometric Ternary Superhydride $LaBeH_8$ as a New Template for High-Temperature Superconductivity at 110 K under 80 GPa. *Phys. Rev. Lett.* **2023**, *130*, 266001

(27) Bi, J.; Nakamoto, Y.; Zhang, P.; Shimizu, K.; Zou, B.; Liu, H.; Zhou, M.; Liu, G.; Wang, H.; Ma, Y. Giant enhancement of superconducting critical temperature in substitutional alloy (La,Ce)H_9. *Nat. Commun.* **2022**, *13*, 5952

(28) Sun, Y.; Wang, Y.; Zhong, X.; Xie, Y.; Liu, H. High-temperature superconducting ternary Li$-R-$H superhydrides at high pressures (R = Sc, Y, La). *Phys. Rev. B* **2022**, *106*, 024519

(29) Chen, S.; Wang, Y.; Bai, F.; Wu, X.; Wu, X.; Pakhomova, A.; Guo, J.; Huang, X.; Cui, T. Superior Superconducting Properties Realized in Quaternary La-Y-Ce Hydrides at Moderate Pressures. *J. Am. Chem. Soc.* **2024**, *146*, 14105–14113

(30) Amri, M.; Clarkson, G. J.; Walton, R. I. Anisotropic Thermal Expansion of SiO2 and AlPO4 Clathrasils with the AST-Type Structure. *J. Phys. Chem. C* **2010**, *114*, 6726–6733

(31) Zhong, X.; Sun, Y.; Iitaka, T.; Xu, M.; Liu, H.; Hemley, R. J.; Chen, C.; Ma, Y. Prediction of Above-Room-Temperature Superconductivity in Lanthanide/Actinide Extreme Superhydrides. *J. Am. Chem. Soc.* **2022**, *144*, 13394–13400

(32) Beekman, M.; Nolas, G. Synthesis and thermal conductivity of type II silicon clathrates. *Physica B* **2006**, *383*, 111–114

(33) Vollondat, R.; Roques, S.; Chevalier, C.; Bartringer, J.; Rehspringer, J.-L.; Slaoui, A.; Fix, T. Synthesis and characterization of silicon clathrates of type I Na_8Si_{46} and type II Na_xSi_{136} by thermal decomposition. *J. Alloys Compd.* **2022**, *903*, 163967

(34) Ammar, A.; Cros, C.; Pouchard, M.; Jaussaud, N.; Bassat, J.-M.; Villeneuve, G.; Duttine, M.; Manatrier, M.; Reny, E. On the clathrate form of elemental silicon, Si_{136}: preparation and characterisation of Na_xSi_{136}(x–>0). *Solid State Sci.* **2004**, *6*, 393–400

(35) Liu, Y.; Briggs, J. P.; Majid, A. A. A.; Furtak, T. E.; Walker, M.; Singh, M.; Koh, C. A.; Taylor, P. C.; Collins, R. T. Formation of Type II Silicon Clathrate with Lithium Guests through Thermal Diffusion. *Inorg. Chem.* **2023**, *62*, 6882–6892

(36) Yamanaka, S.; Komatsu, M.; Tanaka, M.; Sawa, H.; Inumaru, K. High-Pressure Synthesis and Structural Characterization of the Type II Clathrate Compound $Na_{30.5}Si_{136}$ Encapsulating Two Sodium Atoms in the Same Silicon Polyhedral Cages. *J. Am. Chem. Soc.* **2014**, *136*, 7717–7725

(37) Yamanaka, S.; Enishi, E.; Fukuoka, H.; Yasukawa, M. High-Pressure Synthesis of a New Silicon Clathrate Superconductor, Ba_8Si_{46}. *Inorg. Chem.* **2000**, *39*, 56–58

(38) Pena-Alvarez, M.; Binns, J.; Martinez-Canales, M.; Monserrat, B.; Ackland, G. J.; Dalladay-Simpson, P.; Howie, R. T.; Pickard, C. J.; Gregoryanz, E. Synthesis of Weaire-Phelan Barium Polyhydride. *J. Phys. Chem. Lett.* **2021**, *12*, 4910–4916

(39) Laniel, D.; Trybel, F.; Winkler, B.; Knoop, F.; Fedotenko, T.; Khandarkhaeva, S.; Aslandukova, A.; Meier, T.; Chariton, S.; Glazyrin, K.; Milman, V.; Prakapenka, V.; Abrikosov, I. A.; Dubrovinsky, L.; Dubrovinskaia, N. High-pressure synthesis of seven lanthanum hydrides with a significant variability of hydrogen content. *Nat. Commun.* **2022**, *13*, 6987

(40) Semenok, D. V.; Zhou, D.; Kvashnin, A. G.; Huang, X.; Galasso, M.; Kruglov, I. A.; Ivanova, A. G.; Gavriliuk, A. G.; Chen, W.; Tkachenko, N. V.; Boldyrev, A. I.; Troyan, I.; Oganov, A. R.; Cui, T. Novel Strongly Correlated Europium Superhydrides. *J. Phys. Chem. Lett.* **2021**, *12*, 32–40

(41) Li, Z. et al. Superconductivity above 70 K observed in lutetium polyhydrides. *Sci. China: Phys. Mech. Astron.* **2023**, *66*, 267411

(42) An, D.; Duan, D.; Zhang, Z.; Jiang, Q.; Song, H.; Cui, T. Thermodynamically stable room-temperature superconductors in Li-Na hydrides under high pressures. *arXiv preprint* **2023**, arXiv 2303.09805 (accessed 03–06–2024)

(43) Vacanti, A.; Hooper, J.; Altintas, B.; Zurek, E. Metallization of Magnesium Polyhydrides Under Pressure. *Phys. Rev. B* **2013**, *87*, 054107–054107

(44) Sun, Y.; Lv, J.; Xie, Y.; Liu, H.; Ma, Y. Route to a Superconducting Phase above Room Temperature in Electron-Doped Hydride Compounds under High Pressure. *Phys. Rev. Lett.* **2019**, *123*, 097001

(45) Lonie, D. C.; Zurek, E. XtalOpt: an Open-source Evolutionary Algorithm for Crystal Structure prediction. *Comput. Phys. Commun.* **2011**, *182*, 372–387

(46) Falls, Z.; Avery, P.; Wang, X.; Hilleke, K. P.; Zurek, E. The XtalOpt Evolutionary Algorithm for Crystal Structure Prediction. *J. Phys. Chem. C* **2021**, *125*, 1601–1620

(47) Avery, P.; Toher, C.; Curtarolo, S.; Zurek, E. XtalOpt Version r12: An open-source evolutionary algorithm for crystal structure prediction. *Comput. Phys. Commun.* **2019**, *237*, 274–275

(48) Avery, P.; Zurek, E. RandSpg: An open-source program for generating atomistic crystal structures with specific spacegroups. *Comput. Phys. Commun.* **2017**, *213*, 208–216

(49) Lonie, D. C.; Zurek, E. Identifying Duplicate Crystal Structures: XTALCOMP, an Open-Source Solution. *Comput. Phys. Commun.* **2012**, *183*, 690–697

(50) Monkhorst, H. J.; Pack, J. D. Special points for Brillouin-zone integrations. *Phys. Rev. B* **1976**, *13*, 5188–5192

(51) Kresse, G.; Furthmiller, J. Efficient iterative schemes for ab initio total-energy calculations using a plane-wave basis set. *Phys. Rev. B* **1996**, *54*, 11169–11186

(52) Perdew, J. P.; Burke, K.; Ernzerhof, M. Generalized Gradient Approximation Made Simple. *Phys. Rev. Lett.* **1996**, *77*, 3865–3868

(53) Blochl, P. E. Projector augmented-wave method. *Phys. Rev. B* **1994**, *50*, 17953–17979

(54) Hoover, W. G. Canonical dynamics: Equilibrium phase-space distributions. *Phys. Rev. A* **1985**, *31*, 1695–1697

(55) Dronskowski, R.; Blochl, P. E. Crystal Orbital Hamilton Populations (COHP): Energy-Resolved Visualization of Chemical Bonding in Solids Based on Density-Functional Calculations. *J. Phys. Chem.* **1993**, *97*, 8617–8624

(56) Maintz, S.; Deringer, V. L.; Tchougreeff, A. L.; Dronskowski, R. LOBSTER: A tool to extract chemical bonding from plane-wave based DFT. *J. Comput. Chem.* **2016**, *37*, 1030–1035

(57) Togo, A.; Tanaka, I. First Principles Phonon Calculations in Materials Science. *Scr. Mater.* **2015**, *108*, 1–5

(58) Giannozzi, P. et al. QUANTUM ESPRESSO: a Modular and Open-Source Software Project for Quantum Simulations of Materials. *J. Phys.: Condens. Matter* **2009**, *21*, 395502–395502

(59) Methfessel, M.; Paxton, A. T. High-Precision Sampling for Brillouin-Zone Integration in Metals. *Phys. Rev. B* **1989**, *40*, 3616–3621

(60) Allen, P. B.; Dynes, R. C. Transition Temperature of Strong Coupled Superconductors Reanalyzed. *Phys. Rev. B* **1975**, *12*, 905–922

(61) Eliashberg, G. M. Interactions between Electrons and Lattice Vibrations in a Superconductor. *Sov. Phys. JETP* **1960**, *11*, 696–702

(62) Cudazzo, P.; Profeta, G.; Sanna, A.; Floris, A.; Continenza, A.; Massidda, S.; Gross, E. K. U. Electron-phonon interaction and superconductivity in metallic molecular hydrogen. II. Superconductivity under pressure. *Phys. Rev. B* **2010**, *81*, 134506

(63) Wang, C.; Yi, S.; Cho, J.-H. Multiband nature of room-temperature superconductivity in LaH_{10} at high pressure. *Phys. Rev. B* **2020**, *101*, 104506

(64) Di Cataldo, S.; Heil, C.; von der Linden, W.; Boeri, L. $LaBH_8$: Towards high-T_c low-pressure superconductivity in ternary superhydrides. *Phys. Rev. B* **2021**, *104*, L020511

(65) Yao, S.; Song, Q.; Hu, W.; Wang, D.; Peng, L.; Shi, T.; Chen, J.; Liu, X.; Lin, J.; Chen, X. Fermi surface topology and anisotropic superconducting gap in electron-doped hydride compounds at high pressure. *Phys. Rev. Mater.* **2022**, *6*, 034801

(66) Lucrezi, R.; Ferreira, P. P.; Hajinazar, S.; Mori, H.; Paudyal, H.; Margine, E. R.; Heil, C. Full-bandwidth anisotropic Migdal-Eliashberg theory and its application to superhydrides. *Commun. Phys.* **2024**, *7*, 33

(67) Zurek, E.; Hoffmann, R.; Ashcroft, N. W.; Oganov, A. R.; Lyakhov, A. O. A Little Bit of Lithium Does a Lot for Hydrogen. *Proc. Natl. Acad. Sci. U.S.A.* **2009**, *106*, 17640–17643

(68) Shamp, A.; Zurek, E. Superconductivity in Hydrides Doped with Main Group Elements Under Pressure. *Nov. Supercond. Mater.* **2017**, *3*, 14–22

(69) Liang, X.; Bergara, A.; Wang, L.; Wen, B.; Zhao, Z.; Zhou, X.-F.; He, J.; Gao, G.; Tian, Y. Potential High Tc superconductivity in $CaYH_{12}$ under pressure. *Phys. Rev, B* **2019**, *99*, 100505

(70) Hilleke, K. P.; Zurek, E. Rational Design of Superconducting Metal Hydrides via Chemical Pressure Tuning. *Angew. Chem. Int. Ed.* **2022**, *61*, e202207589

(71) Ye, X.; Zarifi, N.; Zurek, E.; Hoffmann, R.; Ashcroft, N. W. High Hydrides of Scandium Under Pressure: Potential Superconductors. *J. Phys. Chem. C* **2018**, *122*, 6298–6309

(72) Nakamoto, Y.; Sakata, M.; Shimizu, K.; Fujihisa, H.; Matsuoka, T.; Ohishi, Y.; Kikegawa, T. Ca-VI: A high-pressure phase of calcium above 158 GPa. *Phys. Rev. B* **2010**, *81*, 140106

(73) Anzellini, S.; Errandonea, D.; MacLeod, S. G.; Botella, P.; Daisenberger, D.; De'Ath, J. M.; Gonzalez-Platas, J.; Ibáñez, J.; McMahon, M. I.; Munro, K. A.; Popescu, C.; Ruiz-Fuertes, J.; Wilson, C. W. Phase diagram of calcium at high pressure and high temperature. *Phys. Rev. Mater.* **2018**, *2*, 083608

(74) Lv, J.; Wang, Y.; Zhu, L.; Ma, Y. Predicted Novel High-Pressure Phases of Lithium. *Phys. Rev. Lett.* **2011**, *106*, 015503

(75) Pickard, C. J.; Needs, R. J. Structure of Phase III of Solid Hydrogen. *Nat. Phys.* **2007**, *3*, 473–476

(76) Chen, Y.; Geng, H. Y.; Yan, X.; Sun, Y.; Wu, Q.; Chen, X. Prediction of Stable Ground-State Lithium Polyhydrides under High Pressures. *Inorg. Chem.* **2017**, *56*, 3867–3874

(77) Mishra, A. K.; Muramatsu, T.; Liu, H.; Geballe, Z. M.; Somayazulu, M.; Ahart, M.; Baldini, M.; Meng, Y.; Zurek, E.; Hemley, R. J. New Calcium Hydrides with Mixed Atomic and Molecular Hydrogen. *J. Phys. Chem. C* **2018**, *122*, 19370–19378

(78) Shao, Z.; Duan, D.; Ma, Y.; Yu, H.; Song, H.; Xie, H.; Li, D.; Tian, F.; Liu, B.; Cui, T. Unique Phase Diagram and Superconductivity of Calcium Hydrides at High Pressures. *Inorg. Chem.* **2019**, *58*, 2558–2564

(79) Mishra, A. K.; Muramatsu, T.; Liu, H.; Geballe, Z. M.; Somayazulu, M.; Ahart, M.; Baldini, M.; Meng, Y.; Zurek, E.; Hemley, R. J. New Calcium Hydrides with Mixed Atomic and Molecular Hydrogen. *J. Phys. Chem. C* **2018**, *122*, 19370–19378

(80) Sun, W.; Dacek, S. T.; Ong, S. P.; Hautier, G.; Jain, A.; Richards, W. D.; Gamst, A. C.; Persson, K. A.; Ceder, G. The thermodynamic scale of inorganic crystalline metastability. *Sci Adv* **2016**, *2*, e1600225

(81) Shamp, A.; Terpstra, T.; Bi, T.; Falls, Z.; Avery, P.; Zurek, E. Decomposition Products of Phosphine Under Pressure: PH_2 Stable and Superconducting? *J. Am. Chem. Soc.* **2016**, *138*, 1884–1892

(82) Drozdov, A. P.; Eremets, M. I.; Troyan, I. A. Superconductivity Above 100 K in PH_3 at High Pressures. *arXiv preprint* **2015**, arXiv:1508.06224 (accessed 04–12–2024)

(83) Bi, T.; Miller, D. P.; Shamp, A.; Zurek, E. Superconducting Phases of Phosphorus Hydride Under Pressure: Stabilization by Mobile Molecular Hydrogen. *Angew. Chem. Int. Ed.* **2017**, *56*, 10192–10195

(84) Fu, Y.; Du, X.; Zhang, L.; Peng, F.; Zhang, M.; Pickard, C. J.; Needs, R. J.; Singh, D. J.; Zheng, W.; Ma, Y. High-Pressure Phase Stability and Superconductivity of Pnictogen Hydrides and Chemical Trends for Compressed Hydrides. *Chem. Mater.* **2016**, *28*, 1746–1755

(85) Errea, I.; Belli, F.; Monacelli, L.; Sanna, A.; Koretsune, T.; Tadano, T.; Bianco, R.; Calandra, M.; Arita, R.; Mauri, F.; Flores-Livas, J. A. Quantum crystal structure in the 250-kelvin superconducting lanthanum hydride. *Nature* **2020**, *578*, 66–69

(86) Belli, F.; Zurek, E. Efficient Modelling of Anharmonicity and Quantum Effects in $PdCuH_2$ with Machine Learning Potentials. *arXiv preprint* **2024**, arXiv:2406.13178 (accessed 07–15–2024)

(87) Yan, Y.; Bi, T.; Geng, N.; Wang, X.; Zurek, E. A Metastable $CaSH_3$ Phase Composed of HS Honeycomb Sheets that is Superconducting Under Pressure. *J. Phys. Chem. Lett.* **2020**, *11*, 9629–9636

(88) Pickard, C. J.; Errea, I.; Eremets, M. I. Superconducting Hydrides Under Pressure. *Annu. Rev. Condens. Matter Phys.* **2020**, *11*, 57–76

(89) McMahon, J. M.; Ceperley, D. M. Ground-State Structures of Atomic Metallic Hydrogen. *Phys. Rev. Lett.* **2011**, *106*, 165302

Graphical TOC Entry